Computer-generated holograms of three-dimensional objects synthesized from their multiple angular viewpoints

David Abookasis and Joseph Rosen

Ben-Gurion University of the Negev, Department of Electrical and Computer Engineering, P.O. Box 653, Beer-Sheva 84105, Israel

Received November 20, 2002; revised manuscript received March 12, 2003; accepted March 18, 2003

Synthesizing computer-generated holograms (CGHs) of a general three-dimensional (3D) object is usually a heavy computational task. We propose and demonstrate a new algorithm for computing CGHs of 3D objects. In our scheme, many different angular projections of computer-designed 3D objects are numerically processed to yield a single two-dimensional complex matrix. This matrix is equivalent to the complex amplitude of a wave front on the rear focal plane of a spherical lens when the object is located near the front focal point and illuminated by a plane wave. Therefore the computed matrix can be used as a CGH after it is encoded to a real positive-valued transparency. When such CGH is illuminated by a plane wave, a 3D real image of the objects is constructed. The number of computer operations are equivalent to those of a two-dimensional Fourier CGH. Computer and optical constructions of 3D objects, both of which show the feasibility of the proposed approach, are described.

OCIS codes: 090.1760, 090.2870, 070.2580, 070.4560, 100.6890.

1. INTRODUCTION

Current approaches to displaying three-dimensional (3D) images can be classified into several main types: stereoscopic display,[1] volumetric system,[2] integral photography[3] (also known as integral imaging), and holography.[4] Each of these technologies has particular advantages and disadvantages. However, holography seems to be a more attractive method of displaying 3D images than others because a single hologram is capable of creating the most authentic illusion of observing volumetric objects by the naked eye. Holographic technology supplies high-quality images and accurate depth cues viewed by human eyes without any special observation devices. However, recording holograms of 3D real objects demands wave interference between two intense laser beams with a high degree of coherence between them.[5] The optical system must be very stable, since a very slight movement can destroy the interference fringes, which contain both intensity and phase information. These requirements, together with the long film exposure[6] and development process, have prevented conventional hologram recorders from becoming widely used for outdoor recording. A partial solution for these limitations might be using computer-generated holograms (CGHs).[7,8] The objects to be constructed by the CGH can be represented in the computer by mathematical or graphical descriptions, or by their spatial samples. The physical interference between light waves is replaced by mathematical computation. However, synthesizing CGHs of 3D images is usually a heavy computational task. This is because one needs to superpose the mathematical contributions of many waves originating from many points on the objects, when not all of them are located at the same distance from the hologram plane.

Many algorithms for synthesizing CGHs have been proposed in the past three decades. The choice among the various algorithms depends on different factors such as computation time, the hologram applications, and image characteristics.[9] In the early days of the CGH, Waters[10] designed a CGH based on the assumption that any object is constructed from many independent light scatterers, each of which is considered as a point source of a parabolic wave front. The superposition of all these complex amplitudes yields the desired complex amplitude distribution on the hologram plane. The depth information is retrievable from continuous parallax and from focusing on different transverse planes through the volume (accommodation effect). The difficulty of this technique comes from the long computation time necessary to superpose waves coming from large number of object points. Ichioka *et al.*[11] reduced the computation time using the "ping pong" algorithm. A method involving the acquisition of objects from different points of view was suggested by Yatagai.[12] His study followed an earlier pioneer work of George and McCrickerd,[13] who had first implemented the technique of the holographic stereogram. Yatagai's hologram has been composed of several Fourier holograms of perspective projections of different 3D objects. In about the same years Yaroslavskii and Merzlyakov[14] also implemented the idea of stereoscopic technique in CGHs. When a viewer looks through such a composite hologram, each of his eyes sees a different perspective of the object, and a 3D display is obtained through the stereoscopic effect. However, the quality of the image cannot be optimal because of the discontinuity between different projections. In another study Frère *et al.*[15] demonstrated a CGH of 3D objects composed of finite line segments. As a result of several conditions and restric-

tions imposed on their reconstruction procedure, Leseberg and Frère[16] later were able to present an improvement of their method in which objects were composed of tilted and shifted planar segments. Tommasi and Bianco[17] proposed to generate an off-axis hologram of tilted and shifted surfaces in the spatial-frequency domain by using translation and rotation transformations of angular spectra. This frequency approach permits the use of the fast Fourier transform algorithm, which decreases the computation time and makes it possible to consider any position of the planes in space. In these last two methods it is necessary to model the object as a series of rotated and translated planes. Lucente[18] invented a more general method called diffraction-specific computation. This method is based on quantizing the space and the spatial frequency of the CGH. In contrast to conventional computation, diffraction-specific computation considers only the diffraction that occurs during the reconstruction of the holographic image. Thus the algorithm permits a trade-off between image quality and computational speed. Adopting Lucente's algorithm, Cameron *et al.*[19] developed a modified version of the algorithm called diffraction specific 1. In this algorithm they have used multiple plane waves to approximate the spherical wave that emanates from a given point in image-volume space. This gives an approximation of the accommodation depth cue. As a result, the human visual system gets the impression of a real point existing in space.

In the present study we suggest a new procedure for generating a CGH of general 3D objects. This procedure creates the CGH by fusing the angular projections of computer-designed 3D objects. Nevertheless, the same algorithm can be employed on a set of angular perspectives of realistic objects captured by a digital camera from some realistic scene, as actually demonstrated in Ref. 20. However, the present algorithm is different from that of Ref. 20, where the scene was observed only from horizontal viewpoints. Here we move the viewpoint in both horizontal and vertical directions. By performing a particular computation on the entire set of angular perspectives of the 3D object, a two-dimensional (2D) complex function is obtained. This function is equal to the complex amplitude of a coherent-light wave front, diffracted from the same object, and then propagates through a spherical lens as far as the rear focal plane. This complex function is then encoded by a conventional procedure to a CGH with real and positive transparency values. Illuminating the CGH by a plane wave reconstructs the original object and creates the volumetric effects. It should be emphasized that, once all the projections are available in the computer memory, the computation complexity of the hologram is equivalent to that of a 2D Fourier transform, and thus the CGH is computed in a relatively short time without sacrificing image quality.

Although the input data in our method are the set of the object's angular viewpoints, our algorithm differs from other algorithms in general and from the stereoscopic[12,14] and multiplex[21] CGHs in particular. Unlike the stereoscopic hologram, our CGH is a single Fourier hologram in which every hologram point contributes a fraction of the light to the entire constructed 3D image, and each point of the constructed image is obtained by light diffracted from the entire CGH. All the angular projections are fused together in a particular mathematical procedure to yield a single Fourier hologram that is equivalent to an optical Fourier hologram recorded by a coherently illuminated 2-f system[22] (but with a 3D object as the system's input). However, the complex wave-front distribution on the Fourier plane is calculated in the computer without any interference experiment. Since the resulting hologram is similar to a Fourier hologram, the reconstruction stage will be carried out by a Fourier lens, as described in the following sections.

The paper is organized as follows. Section 2 describes the new technique of forming the CGH. In Section 3 we show that the proposed technique is a reliable imitation of a specific coherently illuminated holographic system. Computer simulations and experimental results are presented in Section 4. In Section 5 we give conclusions.

2. PROJECTION-BASED ALGORITHM FOR SYNTHESIZING A COMPUTER-GENERATED HOLOGRAM

The first step in our algorithm of synthesizing the CGH is to create in the computer memory a 3D object that later will be reconstructed by this CGH. Next, the set of the object's angular projections are computed. Then a series of mathematical operations are done on the set of projections, the end product of which is a single 2D complex matrix. Finally, the complex matrix is coded to a real and positive-valued matrix to be used as a holographic transparency.

Let us describe this series of steps more rigorously. The object denoted by $t(x_s, y_s, z_s)$ is defined in a Cartesian coordinate system (x_s, y_s, z_s) as shown in the upper part of Fig. 1, where z_s is the longitudinal axis (the virtual optical axis). For each pair of angles ϕ_m, θ_n in the horizontal and vertical directions, respectively, the m, nth perspective of the object is computed. For each ϕ_m, θ_n, the projected image $P_{mn}(x_p, y_p)$ is recorded in the computer memory as a 2D matrix, where (x_p, y_p) is the coordinate system of each projection. With use of well-known geometrical considerations, the relation between (x_p, y_p) and (x_s, y_s, z_s) is given by[23]

$$x_p = x_s \cos \phi_m - z_s \sin \phi_m ,$$

$$y_p = y_s \cos \theta_n - z_s \sin \theta_n \cos \phi_m - x_s \sin \phi_m \sin \theta_n . \quad (1)$$

In the next step of the algorithm, each projected image from the view angle (ϕ_m, θ_n) is multiplied by the exponential function $\exp[-j2\pi b(x_p \sin \phi_m + y_p \sin \theta_n)]$. This product is then summed to get a single complex value in the following way:

$$s(m, n) = \int\int p_{mn}(x_p, y_p) \exp[-j2\pi b(x_p \sin \phi_m + y_p \sin \theta_n)] \mathrm{d}x_p \mathrm{d}y_p , \quad (2)$$

where b is a real-valued constant. The next projected image, viewed from an adjacent point having a small incrementally changed angle, is calculated, and a new value, say $s(m + 1, n)$, is obtained. The values obtained from

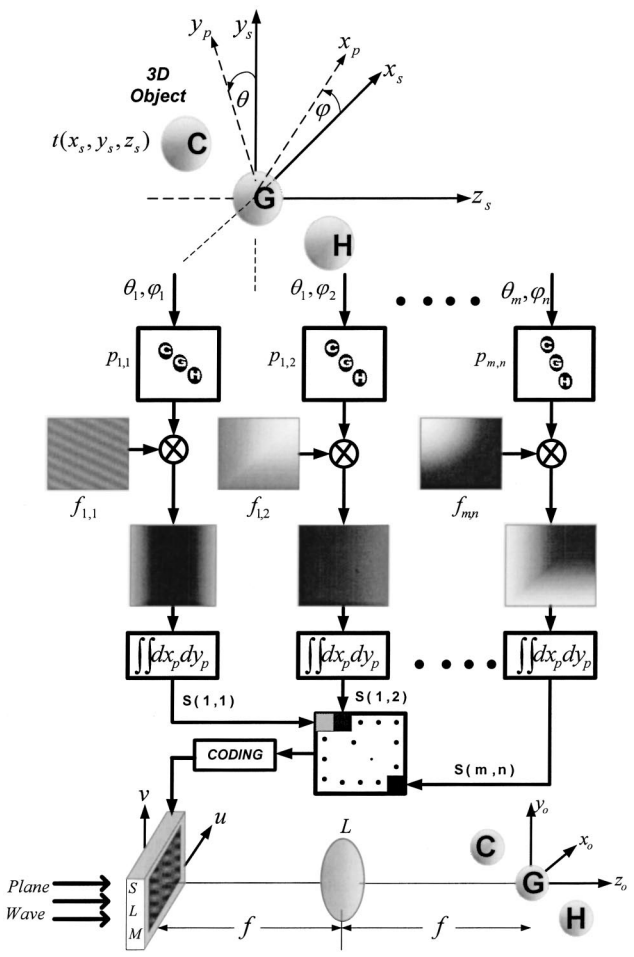

Fig. 1. Schematic of the computational process of the CGH and of the image construction from the CGH. $f_{m,n} = \exp[-j2\pi b(x_p \sin \phi_m + y_p \sin \theta_n)]$.

Eq. (2) are assembled into a complex matrix. Every value of this matrix corresponds to a different point of view and the matrix is arranged in the same order as the projected images are observed. However, as we show later, the connections between the hologram points and the various perspectives exist only in the synthesis stage. In the image reconstruction stage, the resulting hologram is global in the sense that each point of the hologram is radiated onto the entire volumetric image.

Since the matrix values are complex, the hologram must be coded into real and nonnegative values of a holographic transmittance, as described in Section 4. When this coded matrix is coherently illuminated, it yields a holographic reconstruction of the object. The complete computational process is illustrated schematically in the center of Fig. 1; the reconstruction stage is shown in the lower part of the figure. The mathematical verification of this algorithm is described in detail in Section 3.

3. EQUIVALENCE BETWEEN THE ALGORITHM AND RECORDING A FOURIER HOLOGRAM

In this section we show that the proposed CGH algorithm is an imitation of a particular holographic coherent system. Therefore, the constructed image has features similar to those of an image reconstructed from a coherently recorded hologram. The analogy between the optical system and the computation procedure has already been described in detail in Ref. 20 for horizontal projections only. Here the situation is different, and therefore, we analyze the case of bidirectional projections in detail.

Let us look at a single infinitesimal element of size $(\Delta x_s, \Delta y_s, \Delta z_s)$ from the entire 3D object shown in Fig. 1. This element at the point (x_s, y_s, z_s) with value $t(x_s, y_s, z_s)$ appears as a single element on every projection plane (x_p, y_p), but at a different location from one projection to another. Based on Eq. (2), the distribution on the hologram plane for all (ϕ_m, θ_n) values, and for a single source point, is

$$\begin{aligned} s'(m, n) &= \iint t(x_s, y_s, z_s)(\Delta x_s \Delta y_s \Delta z_s)\delta(\bar{x}_p - x_p, \bar{y}_p - y_p)\exp[-j2\pi b(\bar{x}_p \sin \phi_m + \bar{y}_p \sin \theta_n)]\mathrm{d}\bar{x}_p \mathrm{d}\bar{y}_p \\ &= t(x_s, y_s, z_s)\exp[-j2\pi b(x_p \sin \phi_m + y_p \sin \theta_n)](\Delta x_s \Delta y_s \Delta z_s), \end{aligned} \tag{3}$$

where δ is the Dirac delta function. Substituting Eq. (1) into Eq. (3) yields

$$\begin{aligned} s'(m, n) = t(x_s, y_s, z_s)\exp\{-j2\pi b[&\sin \phi_m(x_s \cos \phi_m - z_s \sin \phi_m) + \sin \theta_n(y_s \cos \theta_n \\ &- z_s \sin \theta_n \cos \phi_m \\ &- x_s \sin \phi_m \sin \theta_n)]\}\Delta x_s \Delta y_s \Delta z_s . \end{aligned} \tag{4}$$

Since the input virtual scene is 3D, the overall distribution of $s(m, n)$ resulting from the points of the entire scene is obtained as a volume integral of all the points from the input scene, as follows:

$$\begin{aligned} s(m, n) &= \iiint s'(m, n)\mathrm{d}x_s \mathrm{d}y_s \mathrm{d}z_s \\ &= \iiint t(x_s, y_s, z_s) \\ &\quad \times \exp\{-j2\pi b[\sin \phi_m(x_s \cos \phi_m - z_s \sin \phi_m) \\ &\quad + \sin \theta_n(y_s \cos \theta_n - z_s \sin \theta_n \cos \phi_m \\ &\quad - x_s \sin \theta_n \sin \phi_m)]\}\mathrm{d}x_s \mathrm{d}y_s \mathrm{d}z_s . \end{aligned} \tag{5}$$

The maximum view angles $(\phi_{\max}, \theta_{\max})$ are chosen to be small, and thus the small-angle approximations $\cos \phi_m \approx 1$ and $\cos \theta_n \approx 1$ can be applied. Substituting this approximation in Eq. (5) yields

$$\begin{aligned} s(m, n) \cong \iiint t(x_s, y_s, z_s)\exp\{-j2\pi b[&x_s \sin \phi_m + y_s \sin \theta_n - z_s(\sin^2 \phi_m + \sin^2 \theta_n) \\ &- x_s \sin^2 \theta_n \sin \phi_m]\}\mathrm{d}x_s \mathrm{d}y_s \mathrm{d}z_s . \end{aligned} \tag{6}$$

Under conditions of small view angles, the term $x_s \sin^2 \theta_n \sin \phi_m$ in the exponent of Eq. (6) is much smaller than one radian for the whole range of the variables. Therefore, this term can be neglected. When the matrix

$s(m, n)$ is displayed on any optical transparency, and assuming the angular increment from one projection to another is infinitesimally small, one can change variables of the function s from (m, n) to continuous variables (u, v) as in the following:

$$s(u, v) = \iiint t(x_s, y_s, z_s)\exp\left\{-j4\pi b \frac{\sin\phi_{\max}}{\Delta u}\left[ux_s + vy_s - z_s\frac{2\sin\phi_{\max}}{\Delta u}(u^2 + v^2)\right]\right\}\mathrm{d}x_s\mathrm{d}y_s\mathrm{d}z_s. \tag{7}$$

In deriving Eq. (7) from Eq. (6), we assume that there is an equal angular interval between any two successive projections. In other words, we use the relation $\sin\phi_m = m\sin\phi_{\max}/M$ and $\sin\theta_m = n\sin\theta_{\max}/N$, where M and N are the total number of projections in the horizontal and vertical directions, respectively. It is also assumed in Eq. (7) that the hologram can be displayed on the spatial light modulator (SLM) such that the equality $\sin\phi_{\max}/\Delta u = \sin\theta_{\max}/\Delta v$ is satisfied, where Δu and Δv are the width and the height of the transparency medium, respectively.

It is now shown that $s(u, v)$ of Eq. (7) has the same functional behavior as the complex amplitude on the output plane of the equivalent coherent system shown in Fig. 2. This coherently illuminated setup is the equivalent optical system for the digital process that yields the hologram described in Eq. (7). The 3D object $t(x_s, y_s, z_s)$ is illuminated by a plane wave of wavelength λ, and the reflected wave front from the object propagates through a spherical lens with focal length f. The complex amplitude obtained at the back focal plane is given by[20,24]

$$g(u, v) = C\iiint t(x_s, y_s, z_s)\exp\left\{-j\frac{2\pi}{\lambda f}\left[ux_s + vy_s - z_s\frac{u^2 + v^2}{2f}\right]\right\}\mathrm{d}x_s\mathrm{d}y_s\mathrm{d}z_s, \tag{8}$$

where C is a constant and $g(u, v)$ represents a complex wave front, which should be interfered with a reference wave in order to be recorded as a Fourier hologram. In the case of wave interference, the intensity of the resulting interference pattern keeps the original complex wave front in one of four separable terms.[22] The expressions in Eq. (7) and Eq. (8) are functionally equivalent and the differences exist only in the constants of the exponent

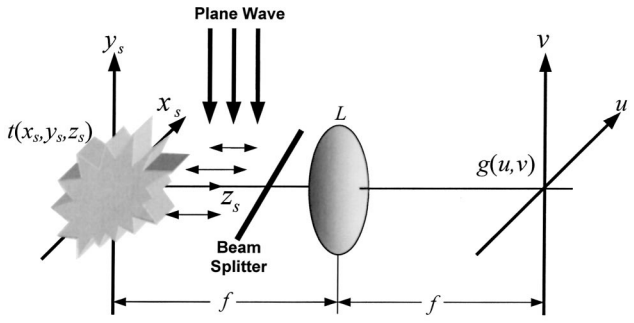

Fig. 2. Equivalent optical system for the CGH computation.

power. Therefore, $s(u, v)$ is a 2D function which contains 3D information of the object similar to the way that a 2D optical hologram contains the 3D information of a recorded object. In both functions $s(u, v)$ and $g(u, v)$, the object's 3D structure is preserved in a holographic manner. This means that light diffracted from the hologram is focused into different transverse planes along the propagation axis according to the object's 3D structure.

This is the right place to re-emphasize that we do not synthesize here a multiplex CGH.[12,14,21] As proved above, the entire reconstructed volumetric image gets light from each point of $s(u, v)$ and the entire distribution of $s(u, v)$ contributes energy to each point on the volume of the reconstructed object. The situation here is definitely dissimilar to the multiplex hologram in which different subholograms generate different 2D images for different viewer perspectives to create all together the effect of a 3D object. The origin of this common confusion, which relates our algorithm to the multiplex hologram, is the similarity in the nature of the input data. The two methods start their computation process from similar input data of multiple perspectives of the object. However, at this point the similarity between the two holograms begins and ends. This is because in our algorithm all of the input perspectives are fused together into a final hologram in which no part can be related to any particular image perspective or any other part of the reconstructed image.

Assuming that the object is constructed by a lens with focal length f and by a plane wave of wavelength λ, the magnifications of the image along the three axes are

$$M_x \equiv \frac{\bar{x}_o}{\bar{x}_s} = \frac{2\lambda f b\sin\phi_{\max}}{\Delta u},$$

$$M_y \equiv \frac{\bar{y}_o}{\bar{y}_s} = \frac{2\lambda f b\sin\theta_{\max}}{\Delta v} = M_x,$$

$$M_z \equiv \frac{\bar{z}_o}{\bar{z}_s} = 8\lambda b\left(f\frac{\sin\phi_{\max}}{\Delta u}\right)^2, \tag{9}$$

where $(\bar{x}_s, \bar{y}_s, \bar{z}_s)$ and $(\bar{x}_o, \bar{y}_o, \bar{z}_o)$ are the sizes of the object in the input space and in the output space, respectively. The ratio between the longitudinal magnification to each transversal magnification is

$$\frac{M_z}{M_x} = \frac{4f\sin\phi_{\max}}{\Delta u} = \frac{M_z}{M_y}. \tag{10}$$

These ratios indicate how much the reconstructed image has been shrunk or stretched along the longitudinal axis in relation to its transverse magnifications.

Equation (7) also gives indications of the desired parameters of the algorithm manifested by Eq. (2). One such parameter is the maximum view angles, which are determined by the spatial bandwidth $(2B_x, 2B_y, 2B_z)$ of the object, according to the following inequalities:

$$b\sin\phi_{\max} \geq B_x, \qquad b\sin\theta_{\max} \geq B_y,$$

$$b(\sin^2\phi_{\max} + \sin^2\theta_{\max}) \geq B_z, \tag{11}$$

where the B_i are in units of $(\text{pixel})^{-1}$. The spatial bandwidth is calculated as the number of cycles of the highest

meaningful harmonic component in the object's composition divided by matrix size. If inequalities (11) are not satisfied, it is expected that high frequencies will be cut off. From these relations it is clear that the parameter b can guarantee that relations (11) are fulfilled for any given bandwidth without increasing the view angle beyond the small-angle limit. Other parameters that should be determined are the angle increments $(\Delta\phi, \Delta\theta)$ between successive projections. Each projection yields a single sample in the Fourier domain, and sampling in the Fourier domain produces replications in the image domain. The angular interval should assure that these constructed replicas do not overlap. Elementary Fourier analysis shows that this sampling condition is fulfilled if

$$(\Delta\phi,\ \Delta\theta) \cong (\Delta \sin\phi,\ \Delta \sin\theta) \leqslant \left(\frac{1}{bW_x}, \frac{1}{bW_y}\right), \quad (12)$$

where (W_x, W_y, W_z) are the sizes of the input object in pixels and $(\Delta\phi, \Delta\theta)$ are in radians.

4. SIMULATED AND OPTICAL CONSTRUCTION OF THREE-DIMENSIONAL OBJECTS

The proposed algorithm was applied on an example of computer-designed 3D objects. The construction stage was demonstrated first by a computer simulation of the system shown in Fig. 1, and then by an optical experiment. The purpose of the computer simulation is to demonstrate the potential quality of the image construction from our method in view of the low quality of the spatial light modulator (SLM) as a holographic transparency. The object used for 3D imaging was composed of three spheres of radius 110 pixels carrying the letters C, G, and H, each of which was located at different depth from the viewer: The C ball was at the back of the scene at point $(x, y, z) = (-170, 170, -170)$ pixels, the G ball was at the center of the scene at point $(x, y, z) = (0, 0, 0)$ and the H ball was at the front of the scene at point $(x, y, z) = (170, -170, 170)$ pixels. From each point of view, a projected image of 700×700 pixels was recorded. The angular range was $\pm 10°$ in all directions with a uniform angular displacement of $\Delta\theta, \Delta\phi = 0.1°$. Nine projections (the central and the eight most extreme) of 201×201 scene viewpoints are shown in Fig. 3. The hologram was computed from this set of 201×201 projections of the 3D scene according to the procedure sketched in Fig. 1. The spectral matrix $s(u, v)$ generated according to Eq. (2) from these data is shown in Fig. 4. The central 100×100 pixels of the magnitude and the phase angle of $s(u, v)$ are shown in Figs. 4(a) and 4(b), respectively.

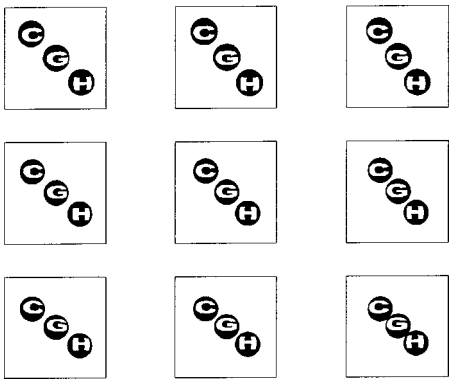

Fig. 3. Nine projections of the 3D objects projected from various viewpoints.

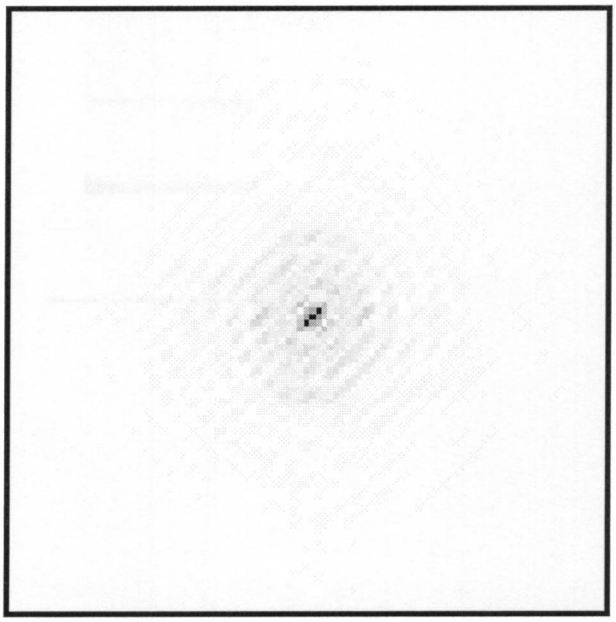

(a)

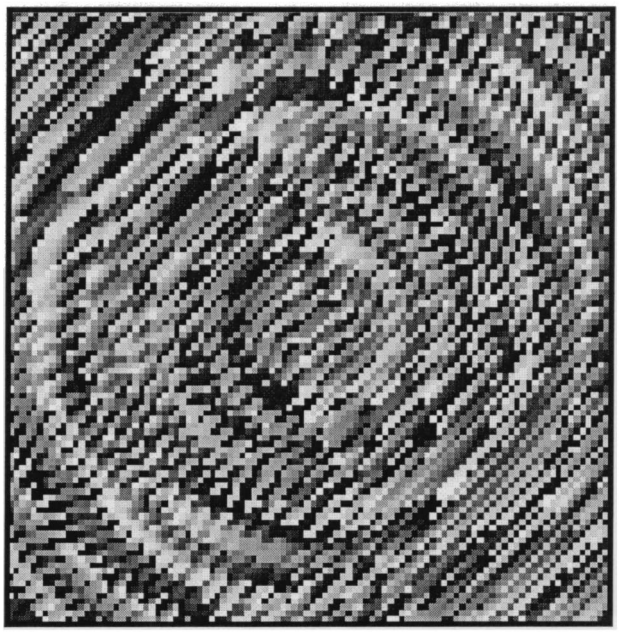

(b)

Fig. 4. Enlarged portion (100×100 pixels of 201×201) of (a) the magnitude and (b) the phase angle of the noncoded CGH generated by the algorithm shown in Fig. 1.

The constructed images from the complex hologram obtained by computer simulation are depicted in Fig. 5.

The contrast of all construction results in this study was inverted for a better visualization. These results are obtained by calculating the diffraction patterns behind a spherical lens at three different transverse planes along the propagation axis z in the vicinity of the rear focal point. These figures show that at each transverse plane, a different letter of a different ball is in focus; thus construction of the 3D objects is demonstrated.

The optical construction from the CGH is also demonstrated. Since the hologram values are stored in the form of the complex function $s(u, v)$, and the SLM used in this study can modulate the light intensity only with positive gray tones, it is necessary to code $s(u, v)$. The complex function $s(u, v)$ was coded into positive, real transparency $T(u, v)$ according to Burch's method[25]:

$$T(u, v) = \frac{1}{2}\left(1 + \mathrm{Re}\left\{s(u, v)\exp\left[j\frac{2\pi}{\lambda f}(d_x u + d_y v)\right]\right\}\right), \tag{13}$$

where (d_x, d_y) is the new origin point of the construction space and $|s(u, v)|$ is normalized between 0 and 1. Some argue that Burch's coding method is not efficient. Our reply is that Burch's method demands much less computation in comparison with other known iterative coding methodes.[21,26,27] Computation is a significant resource which should be considered when one chooses a coding method, especially if the CGH is applied for real-time applications.[20] Moreover, the reconstructed image from such hologram is most similar to the original object. This is because a hologram coded by Burch's method yields in the vicinity of the first diffraction order the exact (neglecting errors caused by a digital sampling and quantization) holographic image of the object. In fact, excluding the zeroth order, Burch's CGH is identical to the conventional optical hologram recorded from the interface between the reference and object beams, and these optical holograms are efficiently useful for many applications. Of course, these comments should not discourage anyone from using or searching for other coding methods that are more efficient in aspects different from those mentioned above, such as diffraction efficiency, space–bandwidth-product, etc. Such alternative methods may even include iterative nonlinear optimization coding methods.[21,26,27] However, this paper is concerned mainly with a new method of computing the complex function $s(u, v)$ from the object function $t(x_s, y_s, z_s)$ rather than in a coding method of the final CGH.

Regarding the diffraction efficiency, we note (see the experiment below) that a slight modification of Burch's method can significantly increase the output diffraction efficiency, defined as the fraction of the total output optical power that appears in the first diffraction order. Disappointingly, however, the overall diffraction efficiency, defined as the fraction of incident optical power that appears in the first diffraction order, is not changed by this modification. This modified method follows the rule

$$T(u, v) = \frac{1}{2}\left(|s(u, v)| + \mathrm{Re}\left\{s(u, v)\exp\left[j\frac{2\pi}{\lambda f}(d_x u + d_y v)\right]\right\}\right). \tag{14}$$

Here the increase in the output diffraction efficiency comes at the cost of an expansion of the zeroth order from a minimal width (inversely proportional to the hologram width) to twice the width of the object. It is clear from this discussion that any improvement of one hologram parameter causes a deterioration of one or more other parameters.

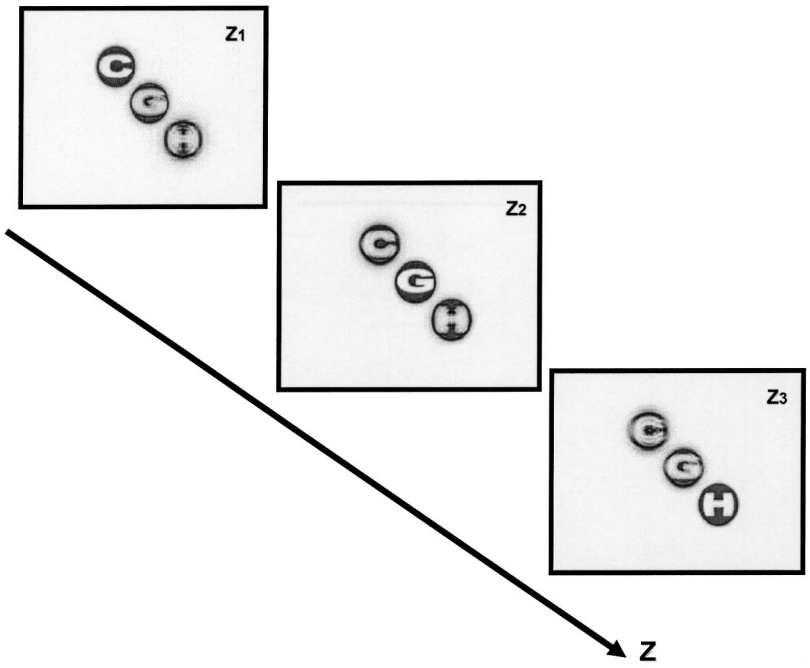

Fig. 5. Simulation results from the hologram shown in Fig. 4 at the vicinity of the back focal plane of lens L for three successive transverse planes along the z axis.

Fig. 6. Central part (300 × 300 pixels of 640 × 640) of the CGH computed by Eq. (13) from the complex function shown in Fig. 4.

The central part of 300 × 300 pixels out of 640 × 640 pixels of the hologram computed by Eq. (13) is shown in Fig. 6. The coded CGH shown in Fig. 6 was displayed on an SLM (CRL, Model XGA1). The total size of the hologram on the SLM is $\Delta u \times \Delta v = 17 \times 21$ mm. To fulfill the condition $\sin \phi_{\max}/\Delta u = \sin \theta_{\max}/\Delta v$, only the central 80% of the original hologram along the u axis is displayed on the SLM. This is equivalent to displaying a hologram in which the maximal view angle along the horizontal direction is 8°, while along the vertical direction the maximal view angle is still 10°.

A collimated beam from a He–Ne laser at 632.8 nm illuminates the SLM and propagates through the spherical lens towards the observer. The real image of the computer-designed, 3D object is constructed in the vicinity of the back focal plane of the lens with a focal length of 750 mm and a diameter of 50 mm. The parameter b in this example was chosen to be equal to 0.9. Figure 7 shows the reconstruction results observed by the CCD (Sony-XC75CE) for three different transverse planes along the optical axis at distances of 715, 750, and 781 mm (±5 mm) from the lens (the distance between the lens and the SLM was 75 mm). The contrast in these figures has also been inverted for better visualization. Obviously, the same effect, in which every letter is in focus at a different transverse plane, also appears in Fig. 7. In comparison with Fig. 5, the construction of the object is noisier; this is due to the use of the SLM and the speckle nature of the laser. SLMs, although they have not reached the technological level of a good holographic transparency, widen the opportunity of implementing dynamic CGHs. This is the main reason that SLM is preferred here over otherwise more suitable holographic transparencies.

The complete diffraction pattern of the hologram is shown in Fig. 8. The three central diffraction orders of

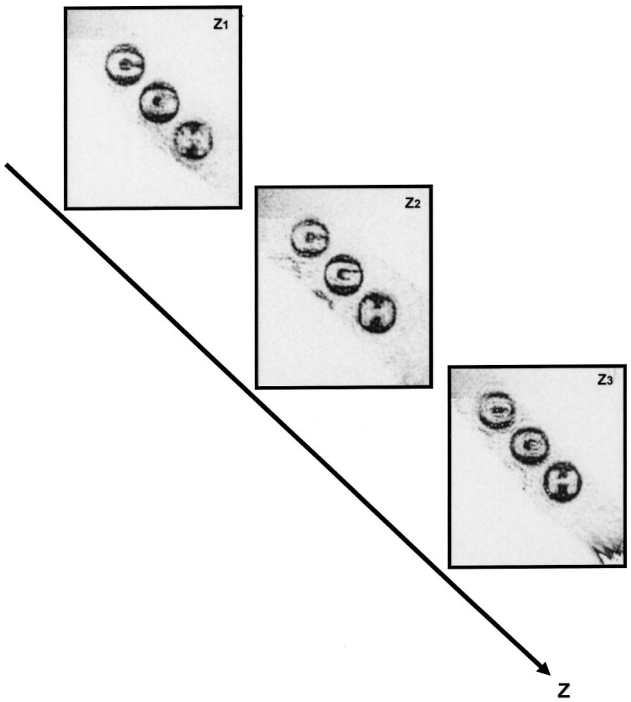

Fig. 7. Experimental results of the first diffraction order obtained from the CGH shown in Fig. 6 at the vicinity of the back focal plane of L for three transverse planes at $z_1 = 715$ mm, $z_2 = 750$ mm, and $z_3 = 781$ mm.

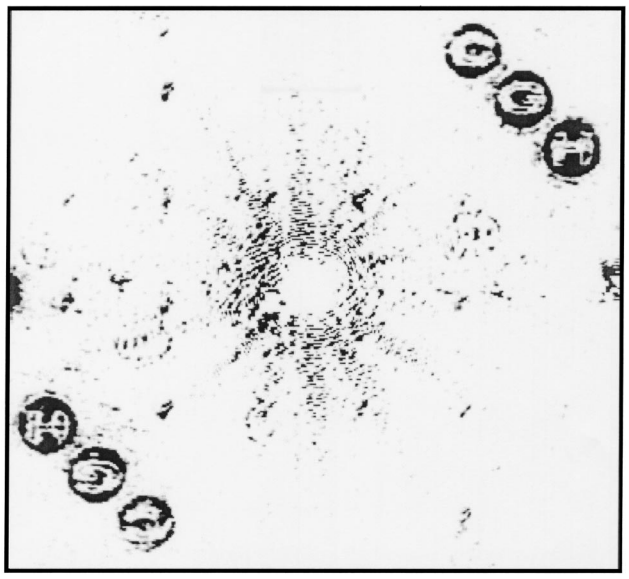

Fig. 8. Construction results from the gray-scale CGH of Fig. 6, including the three central diffraction orders.

the diffracted wavefront can be easily observed. The center of the zeroth order is blocked in Fig. 8 for a clearer visualization. The first diffraction order including the three balls is located in the diagonal direction above the zeroth order.

The overall diffraction efficiency was measured from simulation of the amplitude hologram and found to be 0.0013% in both coding methods given by Eqs. (13) and (14). This figure is typical of this kind of amplitude ho-

logram and could be increased using a phase-only SLM. However, the output diffraction efficiency is dramatically improved from 0.0051% for the hologram coded according to Eq. (13) to 16.7% for the hologram coded according to Eq. (14). The average rms reconstruction error is found to be 0.45%. (For definition of this error, see, for example, Ref. 28.)

To verify the validity of Eq. (10), we compared the theoretical against the experimental ratio of the longitudinal to the transverse magnifications. According to Eq. (10), with the parameters $f = 750$ mm, $\phi_{\max} = 8°$, and $\Delta u = 17$ mm, the ratio between the magnifications is $M_z/M_x = M_z/M_y = 24.6$. On the image captured by the CCD at the back focal plane of the lens, the horizontal and vertical gap between two adjacent balls is 153 pixels. For a pixel size of 8.6 μm and 30 ± 5-mm longitudinal gap between every two successive balls, the experimental magnification ratio is between 19 and 26.6. Therefore, the theoretical result is inside the range of the error measurement.

5. CONCLUSIONS

A new process of computing holograms of computer-designed 3D objects has been proposed and demonstrated. By fusion of multiple projections of the object, a 2D function has been obtained that contains 3D information of the object. The resulting CGH is equivalent to an optical Fourier hologram of a realistic 3D scene. The experimental construction was successfully demonstrated, thus indicating the potential of the technique for 3D displays.

Our study shows that the proposed method has the following features. When the set of projections are available in the computer memory, the rest of the computation is equivalent to the computation of 2D Fourier transforms as manifested by Eq. (2). Therefore, the new method requires less computation time than conventional methods of producing CGHs. This statement should be carefully clarified. Let us assume that the object space contains $N \times N \times N$ pixels. Equation (2) indicates that the number of computational operations is equal to the number of 2D Fourier transform operations only, i.e., N^2 multiplications and summations. [However, since Eq. (2) is not really a Fourier transform, the fast Fourier transform algorithm cannot be applied here.] The number N^2 is significantly less than the number of operations needed in algorithms that suggest direct superposition[10] of all object points in the 3D space, which is of the order of N^3 operations. It is outside the scope of this article to compare the computation complexity of our algorithm with more modern algorithms.[18,19] Such comparison should and probably will be done in the future. In comparison with iterative algorithms,[11,21,26,27] it should be emphasized that our algorithm is noniterative. Therefore its number of computational operations might be compared with them, depending on the number of iterations and the precise details of each iterative algorithm.

Indeed, this discussion ignores the calculations needed for computing the set of angular projections of the 3D object. However, note that memorizing a 3D object in the form of its collection of angular projections is as legitimate as any other form and as exactly compact as the more common form of saving the object's collection of transversal slices. Thus, memorizing 3D objects from the beginning in the form of their angular projections can save a lot of computation later. Alternatively, one can avoid computing the set of angular projections if these projections are recorded by a camera from various viewpoints of a realistic object.[20]

Since the same algorithm can be applied for holograms of realistic 3D scenes, the proposed process may replace part of the traditional holographic recording done by coherent beam interference. In comparison with our previous work,[20] the process is symmetric in both transverse axes. Therefore the volume effects exist in all transverse directions. The process is a reliable imitation of the Fourier holographic coherent system. Therefore, the reconstructed image has features similar to those of an image produced by a coherently recorded Fourier hologram. It should be mentioned that although the method is seemingly limited to Fourier holograms, once the complex wave front on the Fourier plane is computed, any other type of hologram, such as Fresnel or image holograms, can also be computed. This can be done simply by computing the propagation of the wave front from the Fourier plane to any other desired plane by means of Fresnel[8] or near-field[27] operators.

We do not deny that there are several limitations in using the Fourier holograms, among which are the speckle effect and the high space–bandwidth-product requirements. However, the fine results shown in Ref. 19 indicate that there are satisfactory solutions to these problems, even for Fourier holograms. On the other hand, as we mentioned above, our method can be extended to other types, such as Fresnel or image holograms, and this can also be an alternative course for overcoming the limitations of Fourier holograms.

Possible applications of the suggested CGH are in areas where the 3D representation is required. Areas such as computer-aided design, computer graphics, virtual reality, 3D work stations, tomography, and holographic cameras might benefit from the proposed method. Since our hologram is classified as a Fourier hologram, it can also be applied to the areas of object recognition and target tracking in 3D space.[29]

Corresponding author J. Rosen may be reached by e-mail at rosen@ee.bgu.ac.il.

REFERENCES

1. T. Inoue and H. Ohzu, "Accommodative responses to stereoscopic three-dimensional display," Appl. Opt. **36**, 4509–4515 (1997).
2. K. Langhans, D. Bezecny, D. Homann, C. Vogt, C. Blohm, and K.-H. Scharschmidt, "New portable FELIX 3D display," in *Projection Displays*, M. H. Wu, ed., Proc. SPIE **3296**, 204–216 (1998).
3. S.-W. Min, S. Jung, J.-H. Park, and B. Lee, "Three-dimensional display system based on computer-generated integral photography," in *Stereoscopic Displays and Virtual Reality Systems VIII*, A. J. Woods, M. T. Bolas, J. O. Merritt, and S. A. Benton, eds., Proc. SPIE **4297**, 187–195 (2001).
4. S. A. Benton, "Holographic displays: 1975-1980," Opt. Eng. **19**, 686–696 (1980).
5. E. N. Leith and J. Upatnieks, "Wavefront reconstruction

with diffused illumination and three-dimensional objects," J. Opt. Soc. Am. **54**, 1295–1301 (1964).
6. R. J. Collier, C. B. Burckhardt, and L. H. Lin, *Optical Holography*, 2nd ed. (Academic, New York, 1971), Chap. 10, pp. 266–289.
7. A. W. Lohmann and D. P. Paris, "Binary Fraunhofer holograms generated by computer," Appl. Opt. **6**, 1739–1748 (1967).
8. O. Bryngdahl and F. Wyrowski, "Digital holography-computer-generated holograms," in *Progress in Optics*, Vol. XXVIII, E. Wolf, ed. (North-Holland, Amsterdam, 1990), pp. 1–86.
9. P. Hariharan, *Optical Holography*, 2nd ed. (Cambridge, New York, 1996), Chap. 10, pp. 163–177.
10. J. P. Waters, "Holographic image synthesis utilizing theoretical methods," Appl. Phys. Lett. **9**, 405–407 (1966).
11. Y. Ichioka, M. Izumi, and T. Suzuki, "Scanning halftone plotter and computer-generated continuous tone hologram," Appl. Opt. **10**, 403–411 (1971).
12. T. Yatagai, "Stereoscopic approach to 3-D display using computer-generated holograms," Appl. Opt. **15**, 2722–2729 (1976).
13. N. George and J. T. McCrickerd, "Holography and stereoscopy: the holographic stereogram," in *Modulation Transfer Function*, R. R. Shannon and R. J. Wollensack, eds., Proc. SPIE **13**, 342–350 (1969).
14. L. P. Yaroslavskii and N. S. Merzlyakov, *Methods of Digital Holography* (Consultants Bureau, Plenum, New York, 1980).
15. C. Frère, D. Leseberg, and O. Bryngdahl, "Computer-generated holograms of 3-D objects composed of line segments," J. Opt. Soc. Am. A **3**, 726–730 (1986).
16. D. Leseberg and C. Frère, "Computer-generated holograms of 3-D objects composed of tilted planar segments," Appl. Opt. **27**, 3020–3024 (1988).
17. T. Tommasi and B. Bianco, "Computer-generated holograms of tilted planes by a spatial-frequency approach," J. Opt. Soc. Am. A **10**, 299–305 (1993).
18. M. Lucente, "Diffraction Specific Fringe Computation for Electro-Holography," Ph.D. dissertation (Massachusetts Institute of Technology, Cambridge, Mass., 1994).
19. C. D. Cameron, D. A. Pain, M. Stanley, and C. W. Slinger, "Computational challenges of emerging novel true 3D holographic displays," in *Critical Technologies for the Future of Computing*, L. J. Irakliotis, ed., Proc. SPIE **4109**, 129–140 (2000).
20. Y. Li, D. Abookasis, and J. Rosen, "Computer-generated holograms of three-dimensional realistic objects recorded without wave interference," Appl. Opt. **40**, 2864–2870 (2001).
21. J.-N. Gillet, Y. Sheng, "Multiplexed computer-generated holograms with irregular-shaped polygonal apertures and discrete phase levels," J. Opt. Soc. Am. A **19**, 2403–2413 (2002).
22. A. VanderLugt, "Signal detection by complex spatial filtering," IEEE Trans. Inf. Theory **IT-10**, 139–145 (1964).
23. S. Savchenko, *3D Graphics Programming: Games and Beyond* (SAMS Publishing, Indianapolis, Ind., 2000), Chap. 2, pp. 46–53.
24. J. W. Goodman, *Introduction to Fourier Optics*, 2nd ed. (McGraw-Hill, New York, 1996), Chap. 5, p. 104.
25. J. J. Burch, "A computer algorithm for the synthesis of spatial frequency filter," Proc. IEEE **55**, 599–600 (1967).
26. F. Wyrowski, "Diffractive optical elements: iterative calculation of quantized, blazed phase structures," J. Opt. Soc. Am. A **7**, 961–969 (1990).
27. R. Piestun, J. Shamir, B. Webkamp, and O. Bryngdahl, "On-axis computer-generated holograms for three-dimensional display," Opt. Lett. **22**, 922–924 (1997).
28. M. A. Seldowitz, J. P. Allebach, and D. W. Sweeney, "Synthesis of digital holograms by direct binary search," Appl. Opt. **26**, 2788–2798 (1987).
29. Y. Li and J. Rosen, "Object recognition using three-dimensional optical quasi-correlation," J. Opt. Soc. Am. A **19**, 1755–1762 (2002).